FINAL REPORT

Enhanced Oil Spill Detection Sensors in Low-light Environments

Submitted to:

Bureau of Safety and Environmental Enforcement (BSEE)
Oil Spill Response Research Branch

Submitted by:

RDECOM CERDEC, Night Vision and Electronic Sensors Directorate (NVESD)
Special Products and Prototyping Division
10221 Burbeck Road
Fort Belvoir, Virginia 22060-5806

6 June 2018

Acknowledgments

This study was funded in part by the U.S. Department of the Interior, Bureau of Safety and Environmental Enforcement through Interagency Agreement E13PG00031 with the United States Army Research Development and Engineering Command.

Disclaimer

The contents do not necessarily reflect the views and policies of the BSEE, nor does mention of the trade names or commercial products constitute endorsement or recommendation for use.

Table of Contents

Acronyms and Abbreviations

ANS	Alaskan North Slope
BSEE	Bureau of Safety and Environmental Enforcement
C	Cloud Cover
CERDEC	Communications-Electronics Research, Development, and Engineering Center
cm	centimeter
DOD	Department of the Defense
DOI	Department of the Interior
DVE	Degraded Visual Environments
EO/IR	Electro-Optic Infrared
FMC	Forward Motion Compensation
FMV	Full Motion Video
FOV	Field-of-View
FPGA	Field Programmable Gate Array
FPA	Focal Plane Array
FPC	Flexible Printed Circuit
GCP	Ground Control Point
GCS	Ground Control Station
GSD	Ground Sampling Distance
HFOV	Horizontal Field-of-View
h_o	Air Convection Coefficient
HOOPS	Hoover Off-shore Oil Pipeline System
IES	Image Exploitation System
IFOV	Instantaneous field-of-view
InGaAs	Indium Gallium Arsenide
IR	Infrared
k_o	Oil Thermal Conductivity
k_e	Emulsion Thermal Conductivity
K	Cloud Height
L	Crude Oil Thickness
LWIR	Long Wave Infrared

MARINE SCOUT	Mapping and Reconnaissance Imager, Night-Enhanced, for Sensing of Contaminants, Oil, and Unseen Threats
MISA	Miniaturized Integrated Stage Assembly
m	Meter
mm	millimeter
MTF	Modulation Transfer Function
MWIR	Mid Wave Infrared
NVESD	Night Vision and Electronic Sensors Directorate
NIR	Near Infrared
OHMSETT	Oil and Hazardous Materials Simulated Environmental Test Tank
RDECOM	Research, Development and Engineering Command
RH	Relative Humidity
ROI	Regions of Interest
SPPD	Special Products and Prototyping Division of NVESD
SWaP	Size, Weight and Power
SWIR	Short Wave Infrared
T_a	Air Temperature
T_o	Surface Oil Temperature
T_w	Water Temperature
TEC	Thermoelectric Cooler
TTPs	Tactics, Training and Procedures
UAV	Unmanned Aerial Vehicle
UAS	Unmanned Aerial System
V_a	Wind Speed

Figure Captions

Figure 1. Visible image on left showing LWIR camera and crude oil at various millimeter thicknesses (thicker on left column, thinner on right). LWIR image on right taken on 28 April 2017 at 11 AM.

Figure 2. Photograph of the experimental set-up at Ohmsett, showing crude oils contained in 1.5 m diameter rings, blackbody calibration source, and weather station.

Figure 3. LWIR images of three crude oils at various mm thicknesses (thicker on left column, thinner on right). Left (day image) was taken on 12/7/2017 at 9:37 AM, and right (night image) taken at 12/7/2018 at 1:46 AM.

Figure 4. Day and night ANS LWIR thermal images.

Figure 5. Fresh, weathered and emulsified ANS temperatures, along with T_a and T_w during a 24-hour cycle. Data contained in the red circles are at thermal cross over and were not used in the calculations.

Figure 6. Day heat transfer model to predict oil thickness.

Figure 7. An example of day scene temperatures and calculated thicknesses for crude, weathered, and emulsified ANS. The oil depths were calculated using Eq. 6 from ROI temperatures and weather station data.

Figure 8. Night heat transfer model to predict oil thickness.

Figure 9. Night scene temperatures and thickness for ANS crude oil, weathered and emulsified. The oil depths were calculated using Eq. 6 using ROI temperatures and weather station data.

Figure 10. The AeroVironment Puma UAS was selected for this program.

Figure 11. LWIR imagery from a Puma UAV with and without Forward Motion Compensation.

Figure 12. The MARINE SCOUT multi-spectral (NIR/SWIR/LWIR) roll tube.

Figure 13. SWIR Imager spectrum (Left). High-Pass (red) /Low-Pass (green) of the two NIR/SWIR filters (Right).

Figure 14. Custom 11.0 mm F/2.0 lens for NIR/SWIR.

Figure 15. NIR/SWIR filter holder with counterweight (Left). NIR/SWIR imager with lens and paddle filter attached (Right).

Figure 16. Hardware modifications/additions/replacements to the interior of the roll tube assembly.

Figure 17. The initial stages of the MARINE SCOUT PROCESSOR showing data decompression and playback.

Figure 18. Registered stitched maps can be created for all three sensors and viewed simultaneously.

Figure 19. Calibrated LWIR thermal image.

Figure 20. A clutter rejecting mask applied to LWIR map.

Figure 21. Satellite earth imagery of crude oils with legend showing oil depth.

Executive Summary

This document constitutes the final report of Interagency Agreement E13PG00031, between the Department of the Interior (DOI), Bureau of Safety and Environmental Enforcement (BSEE) and US Army Research Development and Engineering Command (RDECOM), Communications-Electronics Research, Development, and Engineering Center (CERDEC), Night Vision and Electronic Sensors Directorate (NVESD). The goal of this collaborative effort is to enhance the methods currently in place to detect oil in a marine environment. The methods currently in place are not conducive to oil spill recovery operations during periods of low light and rely heavily on time-delayed aerial remote sensing technologies, or visual observation. This project leveraged the knowledge and expertise of RDECOM's Night Vision and Electronic Sensors Directorate (NVESD) personnel and assisted BSEE in the identification and documentation of existing capability gaps; identification and assessment of technology gaps; test and evaluate potential new or alternative hardware; and support the design, development and demonstration of new technologies to meet identified needs. The objective of this project involved the design, development and field testing of an unmanned aerial vehicle (UAV) system for day/night remote sensing of oil spills over a marine environment called the "Mapping and Reconnaissance Imager, Night-Enhanced, for Sensing of Contaminants, Oil, and Unseen Threats" (MARINE SCOUT).

Trained oil spill responders can determine the depth of thin layers of crude oil on water by visual inspection. However, catastrophic spills with millimeter (mm) thick oil will just be black, with no visual variation as the oil gets thicker. A day/night heat transfer model was developed to determine crude oil slick thickness. The model uses long wave infrared (LWIR) thermographic imagery, air and water temperature, relative humidity, solar radiation, and wind speed, other weather input such as cloud cover percent and altitudes and measured thermal conductivity of crude oil. Outdoor field-testing was performed at the National Oil Spill Response & Renewable Energy Test Facility (Ohmsett). In April 2017, fresh, weathered, and emulsified ANS crude oils were placed on salt water at mm depths. In December 2017, Alaskan North Slope (ANS), Hoover Offshore Oil Pipeline System Blend (HOOPS), and ROCK crude oils were placed at similar depths. A FLIR camera viewed the scene from a three-story roof-top to simulate UAV altitudes. A low-cost, portable weather station was set up next to the pool and temperature calibrated LWIR imagery was collected day and night. The average oil surface temperature was measured for each target. The day/night model typically predicted oil slick thickness within one or two standard deviations. The fidelity of the thickness measurements is dependent on the accurate measurement of the atmospheric and weather parameters, sea state, heat transfer constants, and calibration and stability of the thermal camera.

MARINE SCOUT is a compact (< 2 lbs.) motion-compensated, multi-spectral sensor with electronics and flash memory data storage. It has full compatibility with the current AeroVironment Puma UAV, while the core technology also is applicable to Group 2 and larger UAS. MARINE SCOUT provides real-time images, works under degraded visual environments (DVE), and provides a measure of extreme oil thickness in marine environments. The airborne payload includes three nadir-stabilized sensor channels derived from two sensor cores. An InGaAs short wavelength infrared (SWIR) sensor is partitioned using spectral filters. Filtered SWIR cameras provide low-light sensitivity, views only surface effects, discriminates against vegetation clutter, and provides good contrast as emulsions have greater reflectivity in the SWIR than the visible. The other sensor

is an uncooled LWIR camera. Based on prior NVESD work, the LWIR camera provided quantitative oil analysis (identification) for >1 mm thick crude oils both day and night. The system incorporates a number of enabling improvements over current EO/IR sensors used on small UAVs, including forward motion compensation (FMC) for improved ground resolvability. The ability to detect oil spills is hindered by image smear due to: forward motion of the platform; very small ground resolvable distances required for reliable detection; long integration times required for imaging under poor illumination conditions; and, the thermal time constant of uncooled LWIR sensors. A solution to the image smear problem uses a novel, FMC enabling technology operating in a nadir-viewing mode. This FMC technology compensates for both the rotational effects of UAV heading and the linear motion apparent in the imagery in the direction of flight, using a compact electro-mechanical assembly on which the imaging sensors are mounted. In addition, onboard image orientation and alignment for precision mosaicing and cross-band/cross-sequence alignment along with near real-time change detection processing are implemented. These capabilities directly support requirements for a mapping capability using high-fidelity, mosaiced, geo-rectified, multi-spectral image stacks (strip maps), and full motion video of contaminated areas. Combined with a ground-based workstation, it allows the oil spill responder to ingest, manage, and view high-resolution, multi-spectral digital imagery and full motion video, and exploit data products using mapping and change detection software. MARINE SCOUT was demonstrated at Ohmsett in December 2017.

Remote measurement of thick oil spill depth using thermal imagery

Introduction

Remote sensing of oil slick thickness (> 1 mm) on water is an active area of research.[1] Although technological advances have been made in the remote detection of oil spills, many of these sensors only provide a single point capability, have limited utility since the sensor is immersed in the water and looks upwards, or do not provide quantitative, real time, thickness measurements for very thick spills at day, night and DVE.[2-6] Thin oil spills are easier to detect as they appear as silvery gray (10^{-4} mm), rainbow (10^{-3} mm), or metallic (10^{-2} mm) sheens, but thick layers appear brown or black. Our goal is to address those operational challenges, enhance remote sensing techniques in a marine environment, and develop tactics, training and procedures (TTPs) for oil spill responders. Under DVE, the LWIR (8-12 μm) spectral region can provide better atmospheric transmission than the visible or near infrared. Previously, we showed that LWIR imagery proved to be a suitable sensor for the identification of mm oil thickness.[7-11] Oil spill detection with uncooled, inexpensive microbolometers is well established, but no quantification of crude oil thickness is available.

A day/night heat transfer model was developed that includes radiation, conduction and convection terms. The day model exploits the heat transfer phenomena that dark crude oils will get hot on a bath of water with sun exposure. It calculates oil thickness (L) from oil surface temperatures (T_o) obtained from a LWIR camera, and air (T_a) and water (T_w) temperatures, solar radiation and wind speed outputs from a weather station datalogger. With solar loading, thicker crude oils will have higher surface temperatures which is proportional to L. At night, contrast is also seen due to the lower emissivity (ε_o) of crude oil versus water (ε_w).[9] Night radiation cooling is included, and is calculated from metrological inputs of cloud cover percent, cloud altitudes, and relative humidity. When implemented into practice, this remote sensing technique can allow oil spill responders to map oil spill thickness in real time.[11]

Experiments

Two outdoor field tests were performed on crude oils and emulsions at Ohmsett. The samples were contained in a target raft containing surface-floating, 1.5 m diameter rings constructed of two-inch, flexible, black poly-pipe (see Figure 1). The target raft was 6.4 m in length and 4.8 m in width and consisted of twelve circular targets in a three-by-four arrangement. Each circular target had a full circumference polymeric skirt that extended 10 to 15 cm below the surface. These skirts did a good job in containing the oils in windy conditions and minimized oil loss and cross contamination.

Alaskan North Slope (ANS) crude oil was used in the April 2017 field test.[12] ANS is a medium grade crude oil that comes from Arctic area where the US has future exploration interests. Fresh, weathered and emulsified ANS was floated on the tank at nominal 10 mm, 5 mm, and 2 mm thicknesses along with sea vegetation (kelp). The weathered crude oil had been used on previous field tests and had lost some high volatility components. The emulsified oils were created prior to the test and had 10% water added by volume. Figure 1 is a picture of the target scene from the prospective of the thermal camera, which was located on an adjacent third story roof top. This location was chosen to mimic the altitude of a UAV that is equipped with a microbolometer LWIR camera. Also shown in Figure 1 is a visible image, with the thicker oil on the left column and the

thinnest on the right. Crude ANS appears on the bottom row, weathered in the middle and emulsified in the third row from the bottom. Submerged kelp is in the top left ring and did not possess a significant thermal signature. Visual inspection of the oil targets cannot determine oil slick thickness.

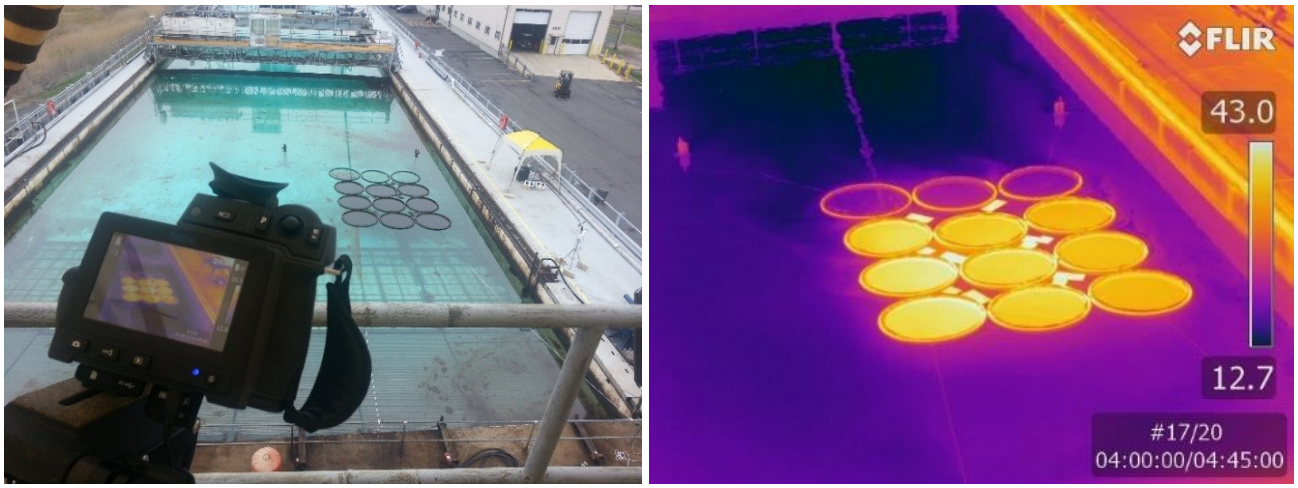

Figure 1. Visible image on left showing LWIR camera and crude oil at various mm thicknesses (thicker on left column, thinner on right). LWIR image on right taken on 28 April 2017 at 11 AM.

Day and night field tests were also performed at Ohmsett in December 2017. Figure 2 is a picture of the target scene showing the crude oils contained on the same stationery target raft as the April 2017 test. Alaskan North Slope (ANS), Hoover Off-shore Oil Pipeline System (HOOPS), and ROCK Crude (Eastern Canada) crude oils were used. Viewing Figure 2, ANS is on the bottom row, HOOPS in the middle, and ROCK Crude in the third row from the bottom. To deliver the desired thickness, the surface area of the ring was calculated and an appropriate volume of oil was measured and delivered with a large graduate cylinder. The thicker (12.5 mm) oils were on the left, 6.25 mm thick in the middle, and thinnest (2.5 mm) on the right. Although the target oil thicknesses are stated above, it should be noted that the spread of oil is very dependent upon a number of variables including degree of weathering, temperature, interfacial tension with the water, viscosity, density, and wind conditions. These factors affect the localized oil thicknesses experienced at any given time. Shown in Figure 3 are typical day and night thermal images.

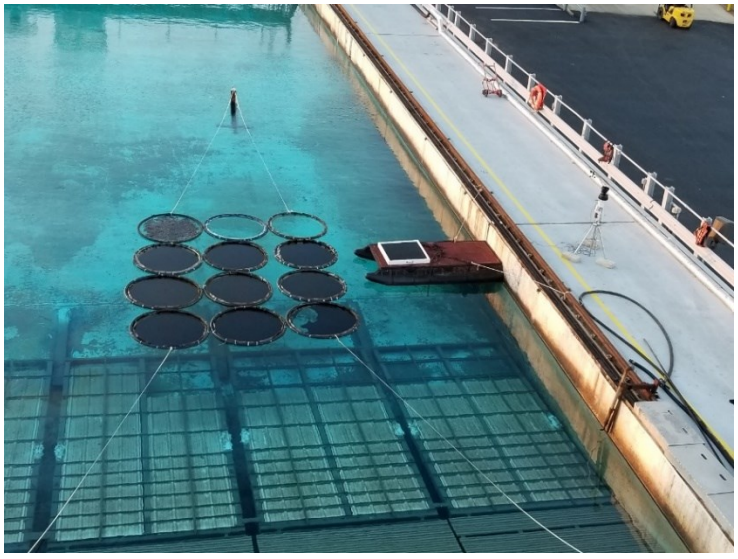

Figure 2. Photograph of the experimental set-up at Ohmsett, showing crude oils contained in 1.5 m diameter rings, blackbody calibration source, and weather station.

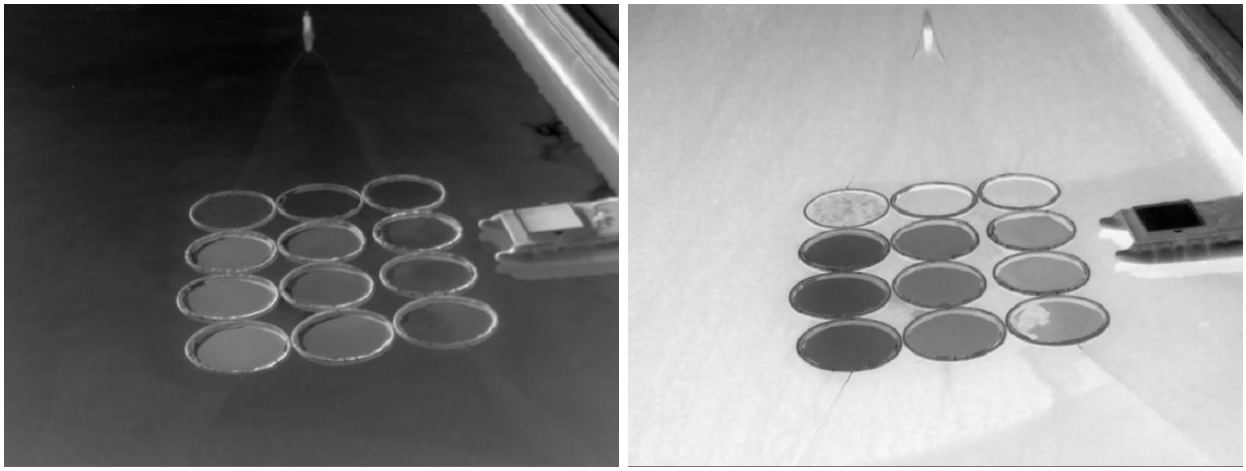

Figure 3. LWIR images of three crude oils at various mm thicknesses (thicker on left column, thinner on right). Left (day image) was taken on 12/7/2017 at 9:37 AM, and right (night image) taken at 12/7/2017 at 1:46 AM.

The FLIR T640SC camera, with 25° field-of-view, viewed the full width of the target raft. The 0.68 milliradian IFOV provided a 1.7 cm GSD at the 25 m standoff range. The quoted thermal sensitivity (NEDT) of the FLIR camera was < 30 mK @ 30^{o}C. Calibrated LWIR imagery was collected for a 24-hour period at 10 or 15 minute intervals. The Onset HOBO H21-USB Micro Station data logger was placed near the target circles and measured T_a, T_w, relative humidity % (RH), solar radiation, and wind speed. The Onset temperature sensors provided < $\pm$ 0.2^{o}C total accuracy and resolution of < $\pm$ 0.03^{o}C over the range of temperatures. Blackbody and water temperature measurements provided useful temperature calibrations during the experiments.

Thermal conductivity (k_o) was measured by Dynalene Laboratory Services for the three oils using transient line heat source methodology. The k_o values were: ANS (0.126 W/m(K)), HOOPS (0.127 W/m(K)) and ROCK (0.135 W/m(K)). For 10% water emulsified ANS, the thermal conductivity (k_e) was estimated to be 0.172 W/m(K).

Results

With sunny conditions, T_o was significantly greater than T_w due to the strong absorption of the black oils and their low thermal conductivity. Temperature differentials ($T_o - T_w$) in excess of 25^{o}C are not uncommon. Thicker crude oils show a larger contrast against water than thinner oils. Emulsified ANS showed smaller temperature differentials due to a higher k_e. At night, the thicker oils were cooler, since ε_o is lower than ε_w and heat transfer was from water to air. Thermal images at various times of day/night appear in figure 4. Thermal cross-over (low image contrast) occurred near 7:00 AM and 6:30 PM for the late April 2017 test and crude oil spill detection, classification, recognition and identification would be poor near sunrise and sunset. Late morning and early afternoon on a sunny day would be the best time to locate crude oil. A rigorous analysis was performed when regions of interests (ROIs) were created and the mean temperatures along with the standard deviations were calculated with Mathcad. The ROI size and location were adjusted to account for raft movements. Shown in figure 5 are ROI day/night ANS temperatures.

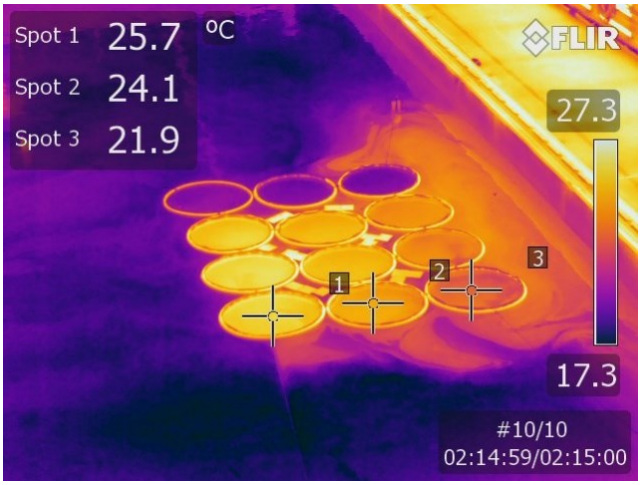

27 April 2017 2 PM

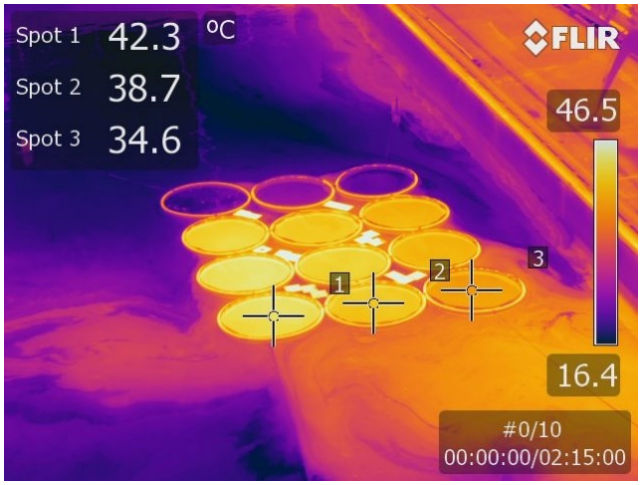

27 April 2017 4 PM

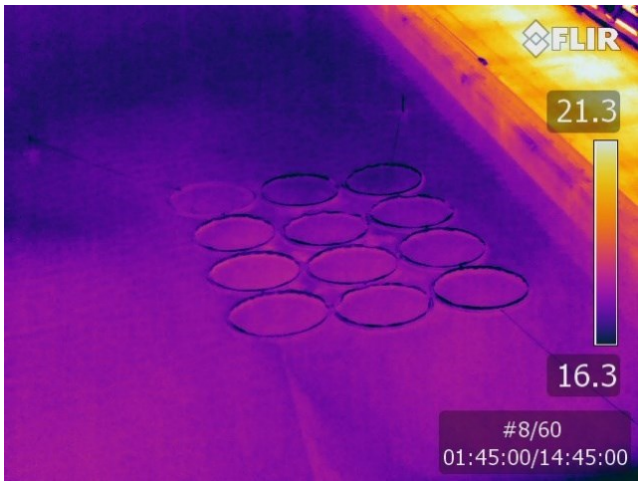

27 April 2017 6 PM

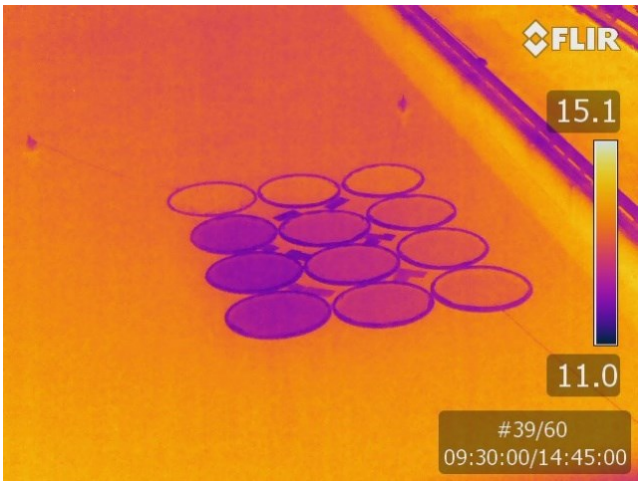

28 April 2017 2 AM

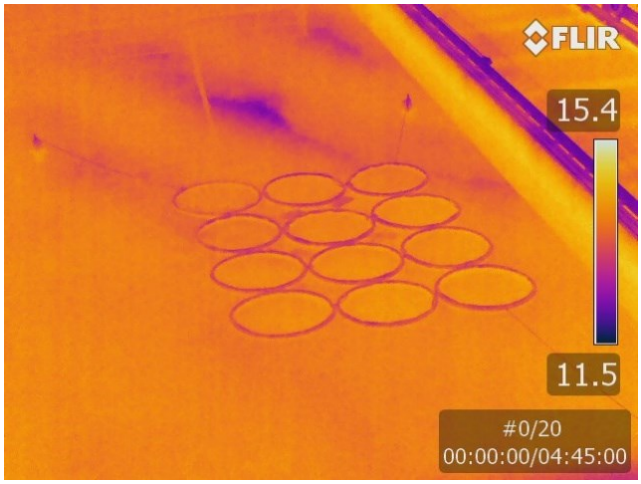

28 April 2017 7 AM

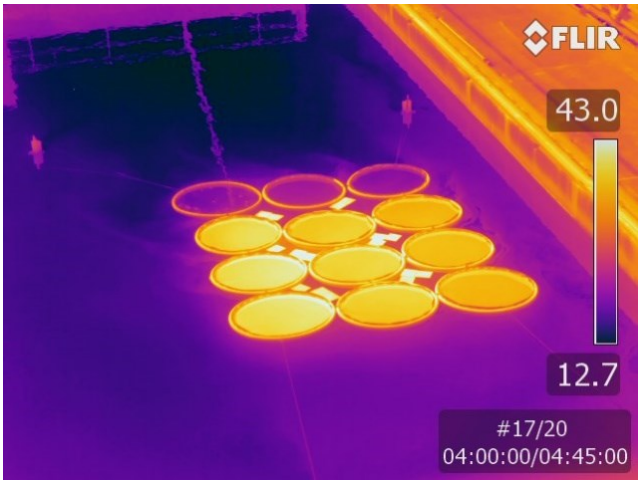

28 April 2017 11 AM

Figure 4. Day and night ANS LWIR thermal images.

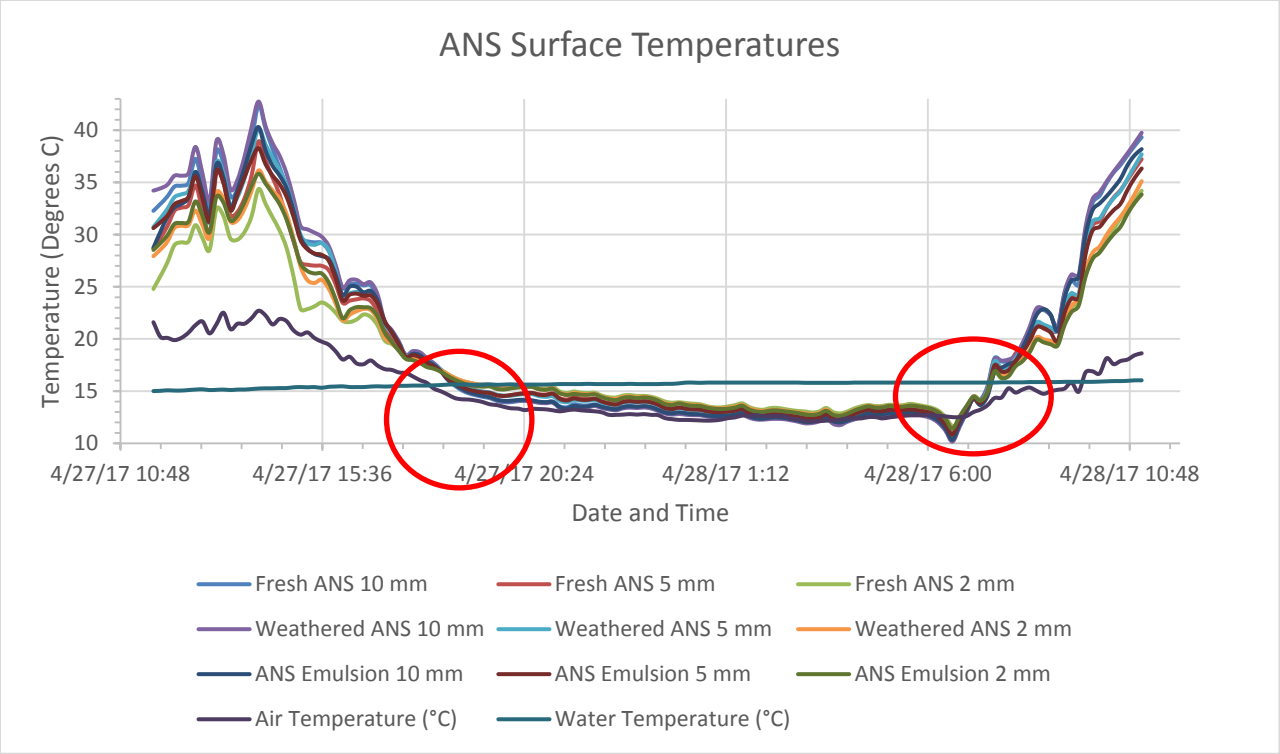

Figure 5. Fresh, weathered and emulsified ANS temperatures, along with T_a and T_w during a 24-hour cycle. Data contained in the red circles are at thermal cross over and were not used in the calculations.

Day Heat Transfer Model

A schematic of the day heat transfer model for mm thick crude oil on water is shown in figure 6. The remote sensing model predicts L using infrared thermography, oil thermal conductivity, and metrological data. In our day model, input solar radiation (E_{in}) heats the oil and the energy is dissipated (E_{out}) through three heat transfer mechanisms: conduction (Fourier's Law), convection (Newton's Law of Cooling) and radiation (Stefan-Boltzmann Law).[13] The heat flux equations, q″ (W/m^2) are the following:

$$q''_{Conduction} = k_o (T_o - T_w)/L \quad \text{(Eq. 1)}$$

$$q''_{Convection} = h_o (T_o - T_a) \quad \text{(Eq. 2)}$$

$$q''_{Radiation} = \varepsilon\sigma(T_o^4 - T_a^4) \quad \text{(Eq. 3)}$$

where ε is the oil emissivity (96%),[9] and σ is the Stefan-Boltzmann constant (5.67×10^{-8} W/m^2K^4). The air convection coefficient (h_o) depends on target geometry, T_o, T_a and air velocity (V_a).[14] For plane surfaces, with length (d_o), h_o is:

$$h_o \cong 1.7\,(T_o - T_a)^{1/3} + 6V_a^{0.8}d_o^{-0.2} \qquad \text{(Eq.4)}$$

Eq. 4 assumes turbulent flow, with the first term accounting for free convection and the second term is forced convection.[14]

For the case where $T_w > T_a$, and applying the conservation of energy ($E_{in} = E_{out}$),

$$\text{Solar Radiation} = k_o\,(T_o - T_w)/\,L + \varepsilon\sigma(T_o^4 - T_a^4) + h_o\,(T_o - T_a) \qquad \text{(Eq. 5)}$$

Rearranging and solving for L, the crude oil thickness is given by Eq. 6:

$$L = \frac{k_o\,(T_o - T_w)}{\text{Solar Radiation} - \varepsilon\sigma(T_o^4 - T_a^4) - h_o\,(T_o - T_a)} \qquad \text{(Eq. 6)}$$

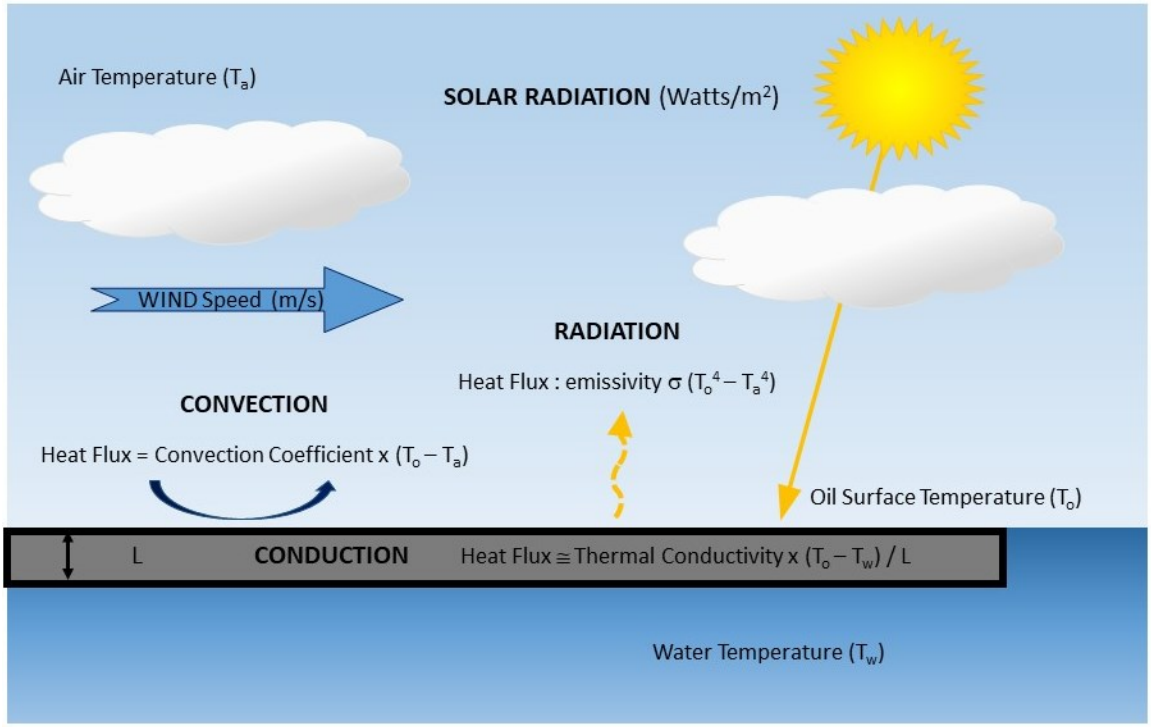

Figure 6. Day heat transfer model to predict oil thickness.

Figure 7 is a sample output for a typical LWIR day scene with ROI overlays for the April 2017 test. During the day, thicker oils have higher temperatures than their thinner counterparts. Emulsified crude oils show less thermal contrast versus thickness than fresh and weathered ANS. This is

attributable to its increased water concentration which yields a higher thermal conductivity. Table I shows the average fresh, weathered and emulsified ANS crude oil thickness and the standard deviations for all (52) day measurements. The results shown in Figure 7 and Table I show very good agreement between calculations and the outdoor field test experiment. The fidelity of the calculation is dependent on the accurate measurement of the experimental parameters, values of the heat transfer constants, and evaporation rate of the crude oil.

Weather Station Outputs

- Solar Radiation (638 W/m^2)
- Air Temperature (16.7°C)
- Water Temperature (15.9°C)
- Wind Speed (1.0 m/s)
- 28 April 2017 (10 AM)

ANS	10 mm	5 mm	2 mm
Emulsion Temperature	38.2°C	36.3°C	33.8°C
Calculated Thickness	7.3 mm	4.7 mm	3.0 mm
Weathered Temperature	39.8°C	37.7°C	35.1°C
Calculated Thickness	7.4 mm	6.6 mm	3.2 mm
Crude Temperature	39.3°C	37.2°C	34.2°C
Calculated Thickness	9.6 mm	4.7 mm	4.2 mm

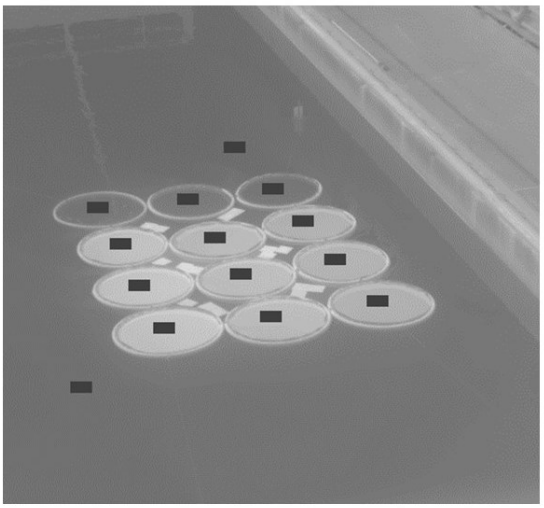

Figure 7. An example of day scene temperatures and calculated thicknesses for crude, weathered, and emulsified ANS. The oil depths were calculated using Eq. 6 from ROI temperatures and weather station data.

Table I. ANS thickness measurements for all day measurements (April 2017).

ANS Crude Oil Sample	Average Thickness (mm)	Standard Deviation
10 mm Fresh	9.6	4.7
5 mm Fresh	5.4	1.8
2 mm Fresh	3.3	1.1
10 mm Weathered	9.9	4.8
5 mm Weathered	9.1	4.5
2 mm Weathered	3.7	1.2
10 mm Emulsified	12.7	6.4
5 mm Emulsified	5.4	1.9
2 mm Emulsified	5.0	1.8

Table II and III summarizes the analysis for the December 2017 test.

Table II. Weather station and average crude oil temperatures used for day oil thickness calculations.

Date, Time - GMT-05:00	Wind Speed	Air Temp	Water Temp	Solar Radiation	ANS 12.5 mm Temp	ANS 6.25 mm Temp	ANS 2.5 mm Temp	HOOPS 12.5 mm Temp	HOOPS 6.25 mm Temp	HOOPS 2.5 mm Temp	ROCK 12.5 mm Temp	ROCK 6.25 mm Temp	ROCK 2.5 mm Temp
Units	**m/s**	**K**	**K**	**W/m^2**	**K**	**K**	**K**	**K**	**K**	**K**	**K**	**K**	**K**
12/7/2017 8:47	2.7	278.3	280.7	208.1	287.0	286.8	286.7	286.2	285.9	285.9	285.7	285.4	285.5
12/7/2017 8:57	3.7	278.2	280.7	229.4	288.0	287.5	287.2	287.2	286.7	286.5	286.8	286.3	286.1
12/7/2017 9:07	3.0	278.6	280.7	249.4	288.6	287.8	287.3	287.8	287.0	286.5	287.4	286.6	286.1
12/7/2017 9:17	2.0	279.0	280.7	265.6	289.7	288.6	287.8	288.9	287.8	287.2	288.5	287.5	286.9
12/7/2017 9:27	2.0	279.2	280.7	283.1	290.4	289.1	288.1	289.7	288.3	287.7	289.0	288.0	287.2
12/7/2017 9:37	2.7	279.5	280.7	304.4	291.0	289.5	288.3	290.2	288.6	287.4	289.9	288.6	287.5

Table III. Results of oil thickness calculations for day measurements.

Date, Time - GMT-05:00	ANS 12.5 mm	ANS 6.25 mm	ANS 2.5 mm	HOOPS 12.5 mm	HOOPS 6.25 mm	HOOPS 2.5 mm	ROCK 12.5 mm	ROCK 6.25 mm	ROCK 2.5 mm
Thickness Units	**mm**	**mm**	**mm**	**mm**	**mm**	**mm**	**mm**	**mm**	**mm**
12/7/2017 8:47	10.2	9.6	9.2	7.7	7.0	7.1	7.1	6.3	6.6
12/7/2017 8:57	21.3	16.1	14.1	14.1	11.2	10.0	12.5	9.8	9.0
12/7/2017 9:07	11.7	8.9	7.7	9.0	7.1	6.0	8.6	6.6	5.8
12/7/2017 9:17	8.6	6.9	5.7	7.4	5.8	5.0	7.1	5.7	5.1
12/7/2017 9:27	8.5	6.6	5.4	7.6	5.7	5.0	7.0	5.7	4.8
12/7/2017 9:37	9.9	7.1	5.6	8.5	6.0	4.6	8.4	6.4	5.0
Average	11.7	9.2	8.0	9.0	7.1	6.3	8.5	6.8	6.0
Standard Deviation	4.8	3.6	3.4	2.6	2.1	2.0	2.1	1.5	1.6

Night Heat Transfer Model

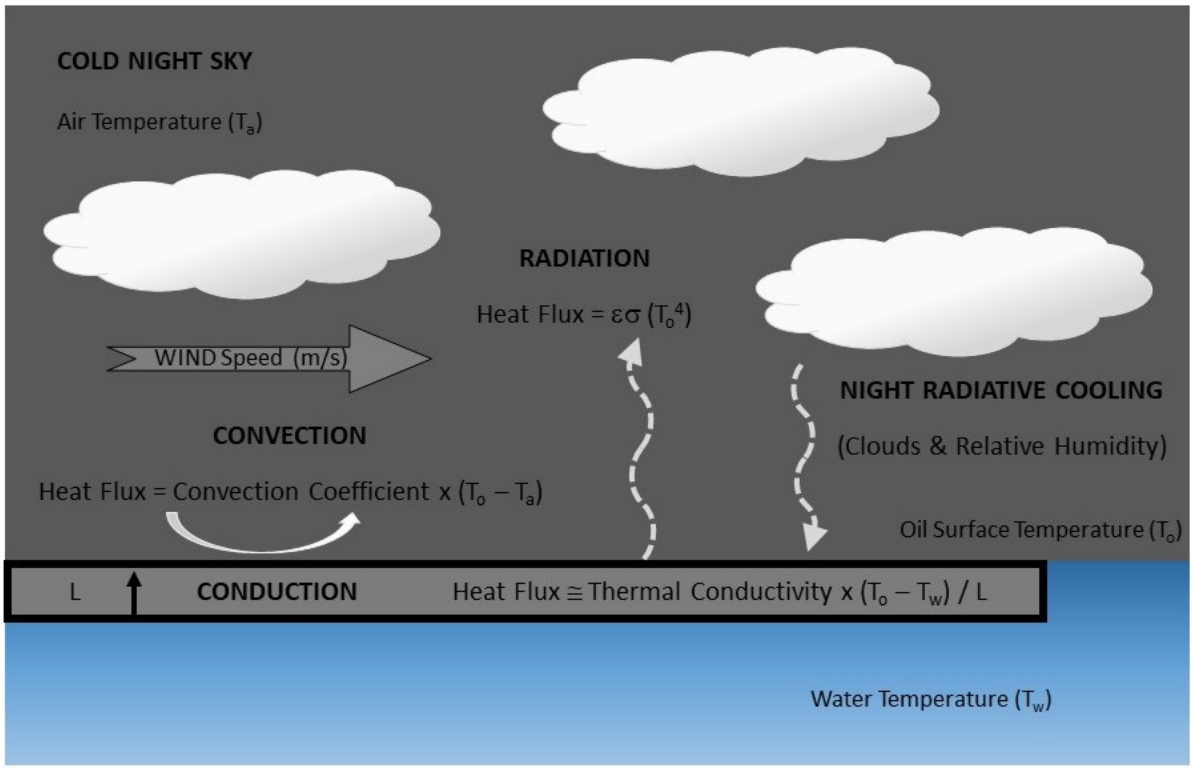

Figure 8. Night heat transfer model to predict oil thickness.

Figure 8 is a schematic of the night model for crude oil depth. Conduction, convection, radiation terms are included in the model along with the modified Swinbank downward thermal night sky radiation, equation (7):[15,16]

$$q''_{\text{Thermal Night Sky}} = [(1 + KC^2) \times 8.78 \times 10^{-13} \times T_a^{5.852} \times RH^{0.07195}] \qquad \text{(Eq. 7)}$$

K is 0.34 for cloud height < 2 km, 0.18 for cloud height between 2 km and 5 km, and 0.06 for height > 5 km. Cloud cover (C) ranges from 0 for clear sky, through 1.0 for totally overcast), and RH is measured in percent.[15,16]

With solar radiation set to zero, $T_w > T_a$, accounting for night radiative cooling, and performing an energy balance, the oil thickness at night is given in Eq. 8.

$$L = \frac{k_o (T_w - T_o)}{\varepsilon\sigma(T_o^4) - [(1 + KC^2) \times 8.78 \times 10^{-13} \times T_a^{5.852} \times RH^{0.07195}] + h_o (T_o - T_a)} \qquad \text{(Eq. 8)}$$

Figure 9 is a sample output for a typical LWIR night scene with ROI overlays for the April 2017 field test. At night, thicker oils have lower temperatures than their thinner counterparts. As with the day measurements, emulsified crude oils show less thermal contrast versus thickness than fresh and

weathered ANS. Night data were encouraging since the difference in T_w and T_o were approximately 1.5°C, but thickness measurements were close to actual values. Table IV shows the average fresh, weathered and emulsified ANS crude oil thickness and standard deviations for 62 night measurements. Once again, very good agreement between the calculations and the outdoor field test. Table V and VI summarizes the analysis for the December 2017 test.

Weather Station Outputs

- Air Temperature (12.6°C)
- Water Temperature (15.8°C)
- Wind Speed (0.7 m/s)
- Relative Humidity (99%)
- 28 April 2017 (2 AM)

ANS	10 mm	5 mm	2 mm
Emulsion Temperature	12.6°C	12.9°C	13.2°C
Calculated Thickness	7.6 mm	6.5 mm	5.3 mm
Weathered Temperature	12.4°C	12.9°C	13.4°C
Calculated Thickness	7.9 mm	6.7 mm	5.6 mm
Crude Temperature	12.6°C	13.0°C	13.5°C
Calculated Thickness	11.0 mm	9.3 mm	8.3 mm

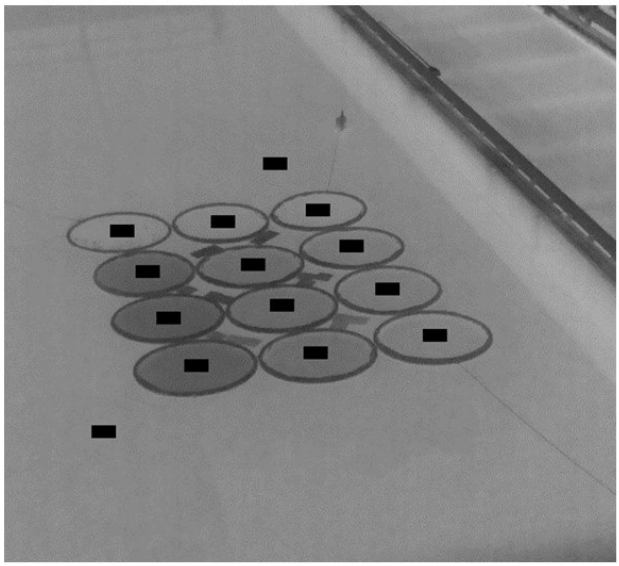

Figure 9. Night scene temperatures and thickness for ANS crude oil, weathered and emulsified. The oil depths were calculated using Eq. 6 using ROI temperatures and weather station data.

Table IV. Summary of ANS thickness measurements using night data.

ANS Crude Oil	Average Thickness (mm)	Standard Deviation
10 mm Fresh	5.8	1.7
5 mm Fresh	4.5	1.8
2 mm Fresh	3.4	1.8
10 mm Weathered	6.0	1.7
5 mm Weathered	4.8	1.8
2 mm Weathered	3.6	1.9
10 mm Emulsified	8.2	2.4
5 mm Emulsified	6.4	2.5
2 mm Emulsified	5.4	2.7

Table V. Weather station and average crude oil temperatures used for night oil thickness calculations for the December 2017 field test.

Date Time - GMT-05:00	Wind Speed	Air Temp	RH	Water Temp	ANS 12.5 mm	ANS 6.25 mm	ANS 2.5 mm	HOOPS 12.5 mm	HOOPS 6.25 mm	HOOPS 2.5 mm	ROCK 12.5 mm	ROCK 6.25 mm	ROCK 2.5 mm
Units	m/s	K	%	K	K	K	K	K	K	K	K	K	K
12/6/2017 22:36	0.3	276.9	48.6	281.3	284.5	274.4	276.0	272.8	274.0	275.4	272.8	274.0	275.3
12/6/2017 22:46	1.3	277.0	47.9	281.2	284.6	274.4	275.9	272.9	274.0	275.3	272.8	274.0	275.1
12/6/2017 22:56	1.3	277.1	47.4	281.2	284.7	274.5	276.0	272.9	274.1	275.3	272.9	274.0	275.2
12/6/2017 23:06	1.7	277.0	47.7	281.2	284.7	274.5	276.0	272.9	274.1	275.3	272.9	274.0	275.1
12/6/2017 23:16	1.7	277.0	47.6	281.2	284.8	274.5	275.9	273.1	274.1	275.4	273.0	274.0	275.2
12/6/2017 23:26	2.0	277.0	47.7	281.2	284.8	274.5	275.8	273.1	274.1	275.3	273.1	274.0	275.1
12/6/2017 23:36	1.3	276.9	48.6	281.2	284.6	274.4	275.9	273.0	274.0	275.3	272.9	274.0	275.2
12/6/2017 23:46	1.7	276.7	48.8	281.2	284.9	274.6	276.1	273.2	274.2	275.4	273.1	274.1	275.3
12/6/2017 23:56	2.0	276.6	49.8	281.2	284.7	274.3	275.8	273.0	273.9	275.1	272.9	273.9	275.0
12/7/2017 0:06	2.0	276.5	50.6	281.2	284.5	274.2	275.7	272.7	273.8	275.1	272.7	273.7	274.9
12/7/2017 0:16	2.3	276.6	50.6	281.2	284.1	273.9	275.4	272.2	273.4	274.7	272.2	273.1	274.5
12/7/2017 0:26	2.3	276.4	51.6	281.2	283.7	273.6	275.1	272.0	273.1	274.6	271.9	273.0	274.4
12/7/2017 0:36	1.7	276.4	51.8	281.2	283.3	273.0	275.0	271.6	273.0	274.4	271.5	272.6	274.3
12/7/2017 0:46	2.0	276.4	52.2	281.2	282.8	272.6	274.6	271.2	272.3	273.9	271.3	272.4	273.8
12/7/2017 0:56	2.3	276.5	52.3	281.2	282.6	272.7	274.6	271.0	272.3	273.8	270.9	272.2	273.7
12/7/2017 1:06	2.0	276.4	52.9	281.1	282.3	272.4	274.5	270.7	272.0	273.8	270.6	272.0	273.5
12/7/2017 1:16	1.3	276.3	53.2	281.1	282.5	272.7	274.6	270.8	272.2	273.7	270.7	272.1	273.6
12/7/2017 1:26	1.3	276.2	54.7	281.1	282.9	272.9	274.7	271.3	272.4	274.1	271.4	272.4	273.8
12/7/2017 1:36	1.3	276.4	54.3	281.1	282.9	273.1	274.8	271.3	272.7	274.0	271.4	272.7	273.9
12/7/2017 1:46	1.3	276.5	54.5	281.1	283.2	273.4	275.1	271.5	272.9	274.4	271.6	272.8	274.2
12/7/2017 1:56	2.3	276.4	55.2	281.1	283.4	273.4	275.2	271.7	273.0	274.4	271.7	272.9	274.3

Table VI. Results of oil thickness calculations for night measurements.

Date Time - GMT-05:00	ANS 12.5 mm	ANS 6.25 mm	ANS 2.5 mm	HOOPS 12.5 mm	HOOPS 6.25 mm	HOOPS 2.5 mm	ROCK 12.5 mm	ROCK 6.25 mm	ROCK 2.5 mm
Thickness Units	**mm**	**mm**	**mm**	**mm**	**mm**	**mm**	**mm**	**mm**	**mm**
12/6/2017 22:46	6.0	4.2	1.1	9.1	5.3	2.3	9.9	5.7	2.7
12/6/2017 22:56	5.9	3.8	0.9	8.7	5.0	2.2	9.5	5.6	2.6
12/6/2017 23:06	5.6	4.0	0.9	9.4	5.1	2.1	10.3	5.8	2.6
12/6/2017 23:16	5.4	3.9	1.0	8.8	5.0	2.0	9.6	5.6	2.5
12/6/2017 23:26	5.2	3.9	1.0	9.3	5.3	2.1	10.3	6.0	2.6
12/6/2017 23:36	5.9	3.8	1.0	8.3	4.8	2.0	8.9	5.3	2.3
12/6/2017 23:46	5.3	3.7	0.9	8.2	4.8	2.0	9.0	5.3	2.4
12/6/2017 23:56	5.1	4.2	1.1	9.3	5.5	2.3	10.1	6.0	2.8
12/7/2017 0:06	5.3	4.4	1.2	10.2	5.8	2.4	10.9	6.4	2.9
12/7/2017 0:16	5.5	4.9	1.1	14.3	7.1	2.5	16.0	8.7	3.2
12/7/2017 0:26	5.8	6.1	1.8	16.5	8.2	3.0	18.1	9.1	3.7
12/7/2017 0:36	6.9	6.6	1.6	14.2	6.8	2.7	15.6	9.0	3.1
12/7/2017 0:46	7.1	8.7	2.2	20.0	10.3	4.0	20.4	10.9	4.5
12/7/2017 0:56	7.2	9.5	2.0	34.3	12.5	4.2	37.9	14.1	4.9
12/7/2017 1:06	7.7	9.1	1.9	27.9	11.8	3.8	31.8	12.9	4.8
12/7/2017 1:16	8.3	6.7	2.0	16.8	8.8	4.0	18.2	9.8	4.5
12/7/2017 1:26	7.7	6.1	1.7	12.9	7.8	3.0	12.9	8.3	3.7
12/7/2017 1:36	7.8	6.3	2.1	14.3	7.6	3.7	14.3	8.0	4.2
12/7/2017 1:46	7.4	5.5	1.5	13.1	7.0	2.9	13.7	7.6	3.5
12/7/2017 1:56	6.1	6.4	1.3	19.7	8.6	3.1	20.4	9.3	3.5
Average	**6.4**	**5.6**	**1.4**	**14.3**	**7.2**	**2.8**	**15.4**	**8.0**	**3.4**
Standard Deviation	**1.0**	**1.8**	**0.5**	**6.9**	**2.3**	**0.8**	**7.7**	**2.6**	**0.8**

Conclusions

A day/night heat transfer model and calculator were developed to determine oil spill thickness. The model uses LWIR thermographic imagery, weather station outputs of air and water temperature, relative humidity, solar radiation, wind speed, other weather input such as cloud cover percent and altitudes, and crude oil thermal conductivity. There are no arbitrary adjustable parameters used in the calculations. The remote thickness measurements with the day/night heat transfer models are typically accurate within one to two standard deviations. The fidelity of the calculation is dependent on the accurate measurement of the experimental parameters, temperature calibration of the LWIR camera, and values of the heat transfer constants. Additional refinements to the heat transfer models may yield more accurate results. The addition of the effects of oil evaporation, water currents and waves to the models would be beneficial.

The day and night models have significant practical application. The implementation of the model will allow oil spill responders to determine oil spill thickness with existing, commercially available thermal radiometric cameras, low-cost weather stations, and observed metrological data. The coverage area can be fairly large and is determined by the sensor pixel pitch and array size, and focal length of the LWIR camera lens and UAV altitude.

Mapping and Reconnaissance Imager, Night-Enhanced, for Sensing of Contaminants, Oil, and Unseen Threats (MARINE SCOUT)

Introduction

Our previous studies showed that LWIR imagery proved to be a suitable sensor for the identification of millimeter oil thickness.[7-11] Oil spill detection with uncooled, inexpensive microbolometers is well established, but no quantification of crude oil thickness is available. Thus, the program named, "Mapping and Reconnaissance Imager, Night-Enhanced, for Sensing of Contaminants, Oil, and Unseen Threats" (MARINE SCOUT) was initiated. During 2017, two airborne sensor payloads as well as a ground processing capability were developed and subsequently tested and evaluated for their ability to map the ground in a precision, image-stabilized scan pattern, detect the presence of crude oil, and measure oil spill thickness. The airborne payloads are compatible with the AeroVironment Puma UAS (Figure 10) and represent unprecedented multispectral sensing and digital mapping capability in a small (< 2-lb), multi-axis stabilized payload.

Figure 10. The AeroVironment Puma UAS was selected for this program.

Operational and Capability Description

MARINE SCOUT combines a compact (< 2 lbs.) motion-compensated, multi-spectral sensor with onboard electronics and digital data storage. The system design was based on a prior Army project supporting route reconnaissance, and the two fabricated MARINE SCOUT payloads were built upon available hardware from that project, with new sensors, optics, and supporting hardware/firmware/software developed to support the oil detection application. MARINE SCOUT has full compatibility with the AeroVironment Puma UAS, while the core technology also is applicable to Group 2 and larger UAS. The custom, miniaturized reconnaissance-type payload has two basic modes of operation:

- **Mapping (or Reconnaissance) Mode** – system is viewing at or near nadir, while multispectral, digital image mosaics are collected of the earth surface (water and/or terrain). The strip-map

type imagery is collected in step-stare fashion, with three spectral channels collected using only two imagers (one of which has a filter paddle, as described below).

- **Full Motion Video (FMV) Mode** – system can view on- or off-nadir (but most typically would be off-nadir and side viewing), while one of the three sensor channels, selectable, is transmitting FMV for situational awareness.

MARINE SCOUT provides real-time video, works under DVE, and provides a measure of extreme oil thickness in marine environments. The airborne payload includes three nadir-stabilized sensor channels derived from two sensor cores. An InGaAs detector based NIR-SWIR focal plane array (FPA) is used in conjunction with a spectral filter paddle to separate the NIR and SWIR channels, collected in sequential interleaved frames. The filtered SWIR camera provides partial low-light sensitivity, senses only marine surface effects, provides good contrast as emulsions have greater reflectivity in the SWIR than the visible-NIR, and discriminates oil products from vegetative clutter by processing the ratio of the SWIR to NIR response at each swath of collected imagery.[7-9] The other sensor is an uncooled LWIR camera that provides a quantitative oil sensing measurement for >1 mm thick crude oils both day and night. The system incorporates a number of enabling improvements over current EO/IR sensors used on small UAVs, including FMC for improved ground resolvability. The ability to characterize oil spills is hindered by image smear due to: forward motion of the platform; very small ground resolvable distances required for reliable detection; long integration times required for imaging under poor illumination conditions; and the thermal time constant of uncooled LWIR sensors. A solution to the image smear problem uses a novel, enabling technology for accomplishing FMC operating in a nadir-viewing mode. This FMC technology compensates for both the rotational effects of UAV heading and the linear motion apparent in the imagery in the direction of flight, using a compact electro-mechanical assembly on which the imaging sensors are mounted. In addition, the payload has onboard electro-mechanical image orientation and alignment for precision mosaicing and cross-band/cross-sequence alignment. These capabilities directly support requirements for mapping using high-fidelity, mosaiced, geo-rectified, multi-spectral image stacks (strip maps), and full motion video of contaminated areas. Combined with a ground-based workstation, it allows the oil spill responder to ingest, manage, and view high-resolution, multi-spectral digital imagery and full motion video, and exploit data products using processing and mapping software.

The NIR/SWIR and LWIR sensor cores are mounted to a precision linear motion stage. Both sensor cores on their respective linear motion stages are mounted atop synchronous rotary stages that orient the imagers to the measured heading of the aircraft so that the linear stages move in the axis of flight and scene motion. The linear and rotary motion stages are integrated together in a unit referred to as the Miniaturized Integrated Stage Assembly (MISA), that in whole performs the FMC which was a key enabling technology developed under the legacy Army program. The FMC enables high-resolution imaging (i.e. minimal image blur due to forward motion of the platform) of the ground and objects on the ground from a low flying UAV using compact, affordable sensors (Figure 11).

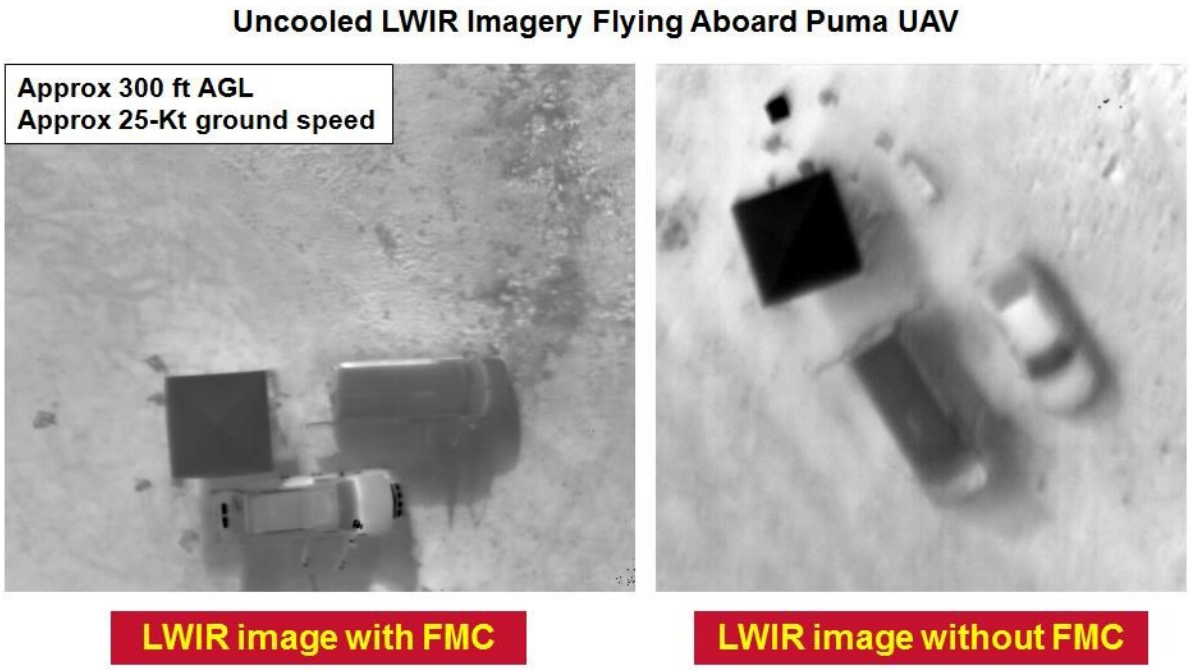

Figure 11. LWIR imagery from a Puma UAV with and without Forward Motion Compensation.

To reduce the risk of payload damage during landings, protect against dust/dirt and water contamination, etc. the optical bench and all camera electrical and optical components are housed within a sealed roll tube. The roll tube is mounted within a standard modular Puma payload container that is approximately 10" x 4" x 6" in size. The entire MARINE SCOUT payload mounts into the Puma fuselage and replaces the standard gimbaled Puma EO/IR camera payload. The MARINE SCOUT payload interconnects to the Puma via a flexible printed circuit (FPC) cable. The payload is controlled using the Puma's common ground control station (GCS). The GCS is the primary aircraft/payload controller and also allows the operator to operate the aircraft manually or program it for GPS-based autonomous navigation.

During takeoff, with the MARINE SCOUT payload mounted in the Puma fuselage, the roll tube is stowed such that the sensors are oriented upward and are protected within the fuselage from damage during landing and against dust/dirt and water contamination. During flight operations, the pilot commands the roll tube to be activated which rotates the roll tube to the downward looking position such that the sensors are staring through the opening in the fuselage at the earth below and able to record multi-spectral (NIR/SWIR/LWIR) imagery. During landing operations, the pilot commands the roll tube to be stowed which rotates the roll tube upward such that the camera apertures are facing upward and protected from damage during landing. Shown in Figure 12 is the MARINE SCOUT multi-spectral roll tube.

Figure 12. The MARINE SCOUT multi-spectral (NIR/SWIR/LWIR) roll tube.

The key capability objectives of the MARINE SCOUT Program are enumerated in Table VII.

Table VII. MARINE SCOUT Capability Objectives

Enhancement	**(a) Airborne Payload**
Forward Motion Compensation (FMC) & Pointing	• Linear stage eliminates image smearing for improved resolution in mapping the water/land. • Rotary stage compensates image skew due to yaw-angle effects (platform crabbing) at nadir. • Outer gimbal maintains nadir or off-nadir line-of-sight pointing in presence of platform roll.
High-Fidelity Multispectral Digital Sensors	• True day/night capability using high-dynamic range digital uncooled thermal IR camera. • Dual-band NIR-SWIR using high-dynamic range digital InGaAs sensor & filter paddle. • Custom optics providing high throughput, wide FOV, and low distortion over the full FOV.
Enhanced Digital Data Link (DDL)	• Digital imagery transmission improves resolution, dynamic range & sensitivity vs. analog. • Tailored DDL link can simultaneously transmit digital imagery and full motion video (FMV).
On-board Native Data Storage	• Real-time, lossless storage of digital imagery robustly accommodates communication issues (e.g., unpredictable performance in the DDL) using a store–and-forward paradigm.
Enhancement	**(b) Ground Station**
Quasi-Radiometric Calibration	• Sensors are not radiometrically calibrated, so software performs an in-scene projection using water temperature estimation and other sources, when available (e.g., test blackbodies).
Visualization & Manipulation	• Display, manipulate, and compare multispectral / multi-pass mosaics. • Generate reports for forensics, analysis.

Airborne Payload Description and Development Effort

Overview

The development effort started with a legacy Army payload, with a requirement to modify the sensor channels to optimize performance for the oil spill sensing and mapping mission. In addition to modifying the reflective band sensor channels, the effort included reconstituting CAD models and recreating the firmware and software development environments from the original project.

Leveraging prior research.[7-9] performance specifications and payload attributes were established to address the maritime oil spill characterization mission. The sensor channels required wider fields of view (FOV) to capture as much scene as possible during each airborne pass. A dual-band SWIR sensor was deemed necessary to provide the NIR and SWIR sensor channels, augmented by an existing LWIR sensor core to sense and discriminate oil. This required modifying the legacy payload with new lenses, replacing one of the sensors for an extended range SWIR imager, and adding a filter toggling mechanism to cover both the SWIR and the NIR bands. The technical challenge was to fit these design elements into the existing Size, Weight and Power (SWaP) envelope and architecture of the existing payload.

A trade study was performed on available SWIR imagers that fit the strict performance and SWaP requirements of the system, while imaging over the NIR and SWIR spectrum. In the end, there were not many sensors that fit the criteria, and a Sensors Unlimited 640CSX with extended range was identified and chosen. In parallel, an investigation into lenses quickly made it apparent that two new custom lens designs would be necessary to meet the objectives of matching wide field of views for all three bands over the desired performance. Additional hardware modifications included adding a filter changer into the system. Considerations of size and power with the required torque and speed to keep up with the flight speeds led to the choice of a miniature, bi-stable solenoid to toggle a custom dual filter mount. A driver board was necessary to operate the solenoid and had to be customized to fit into the size constraint. All of these additions required unique mechanical designs to fit into tight spaces while not hindering payload operation or installation. Additionally, the firmware and software had to be updated to incorporate all these hardware changes into the functionality of the system. This included control system modifications and development, image capture/toggling synchronization, adjustments for the new camera, and more.

Optics and Spectral Filters

The dual-band NIR/SWIR imager was coupled to a custom 11-mm, F/2.0 lens with several design challenges: i) maintain a back focal length to allow clearance for the switching filters between last lens and focal plane array, ii) retro-fit into an existing very compact structure, iii) color correction from 500 to 1700 nm, and iv) remain focused over the operating temperature range expected for ocean environments from the arctic to the tropics. Figure 13 portrays the sensor spectral response and the desired dual bands covering the NIR and SWIR.

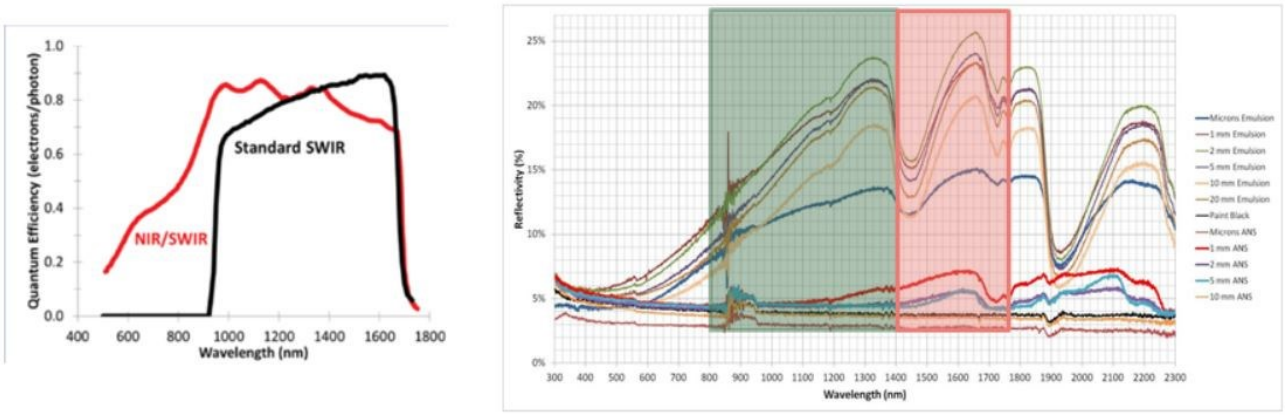

Figure 13. SWIR Imager spectrum (Left). High-Pass (red) /Low-Pass (green) of the two NIR/SWIR filters (Right).

Even though this could be considered a normal lens (HFOV=40°) for the size of the focal plane array, the end design involved a compromise between field curvature and moderate distortion while maintaining athermalization, good color correction, and sufficient MTF to match the pixel pitch of 12.5 µm. Heat removal from the FPA was facilitated by an MTEQ manufactured flexible high thermal conductivity ribbon to allow free functioning of the FMC mechanism.

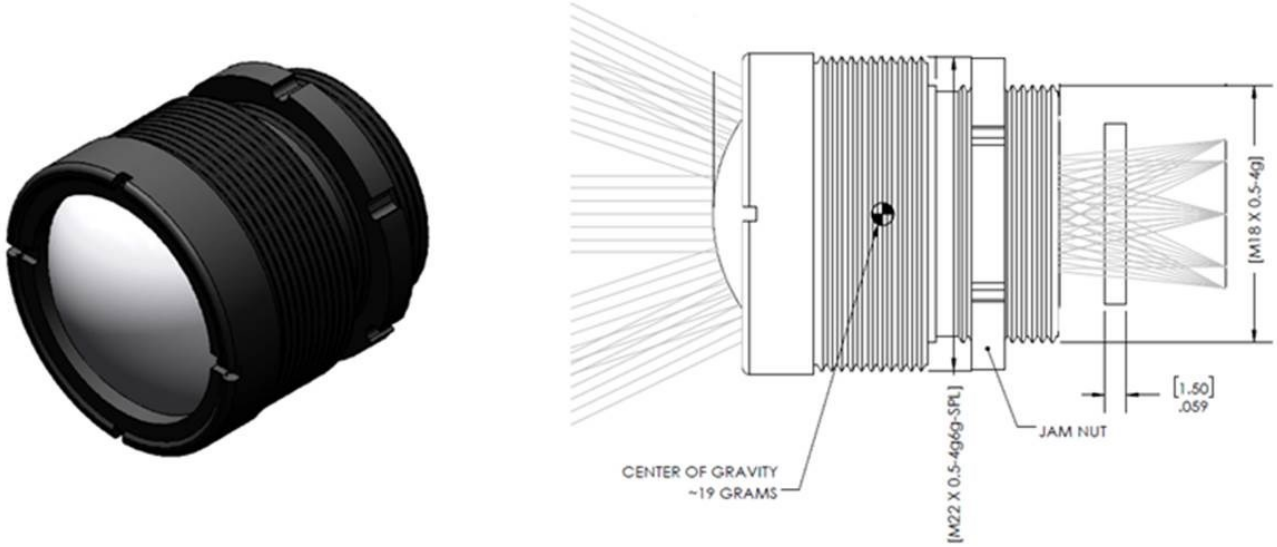

Figure 14. Custom 11.0 mm F/2.0 lens for NIR/SWIR.

Bispectral images from the NIR/SWIR imager were achieved by rapidly switching between two 12.5 mm dia. filters, the first with a passband from 660 to 1400nm (Edmund Optics 84-644) and the second with a passband from 1400 to 2000 nm (custom filter). The low amount of lateral color of the lens (<0.5 pixel over image circle) made for nearly indiscernible changes between images in either passband.

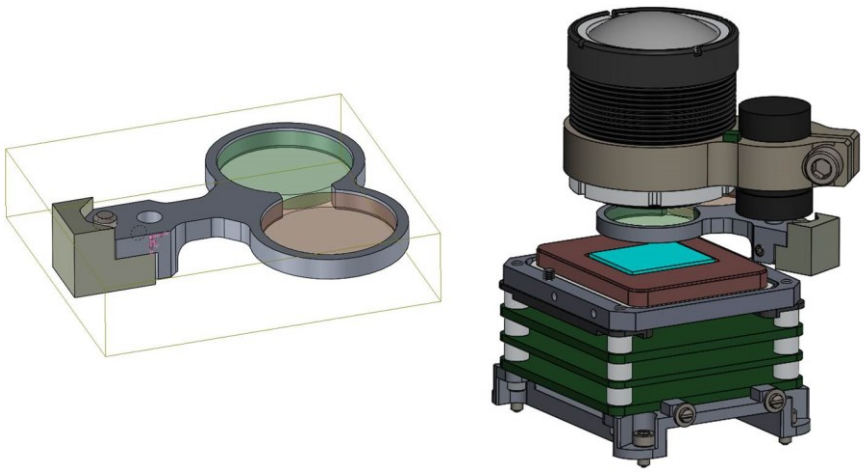

Figure 15. NIR/SWIR filter holder with counterweight (Left). NIR/SWIR imager with lens and paddle filter attached (Right).

The LWIR imager, a custom 15 mm F/1.0 lens with an identical HFOV of 40° when mated to its uncooled focal plane array (FLIR Quark), faced the same challenges, except no switching filter. However, that lens was required to match distortion of NIR/SWIR optical path to achieve optimum pixel co-registration over the entire operating range.

Sensors & Firmware

The two system sensors are the Sensors Unlimited 640CSX Micro SWIR with extended range, covering the NIR and SWIR bands, and the FLIR Quark covering the LWIR. A new PCB flex cable and corresponding interface board was designed to integrate the NIR/SWIR sensor into the system and a motor driver board was designed to move the rotary bi-stable solenoid controlling the paddle filter. Some reverse engineering of the existing electronics was performed to tap into the existing architecture to control the solenoid driver board.

Regarding firmware and software, the full development environments had to be recreated to support design changes, and cover all new efforts to build, compile, program, flash and image the two FPGAs and embedded soft-core microprocessor. The updated firmware and software functionality included a separate build for updating the factory calibration of the LWIR camera, due to the hypersensitivity to the roll tube environment. Modifications also included command and control for the SWIR camera, control loop updates to control and synchronize the paddle filter, adjusting the video capture and forward paths to compensate for the new camera resolution and pixel clock speed, as well as FMC image capture control system updates for the heavier SWIR sensor and wider field of view.

Mechanical Modifications

Inside the MARINE SCOUT sensor roll tube, a number of components were added, modified, or replaced from the legacy sensor system without increasing the overall size or sacrificing existing capabilities. The NIR/SWIR camera sensor, and custom printed flexible cable directly replaced their respective legacy components, requiring a new custom mount made of Invar to minimize the effects of thermal expansion. The NIR/SWIR filter switching assembly was added to the space between the lens and sensor, uniquely attached by mounting straight to the lens. The filter assembly and

counterweight are toggled by a bi-stable solenoid, which requires a custom driver board. To avoid operational interference, this had to be mounted to an end cap. The NIR/SWIR sensor utilizes a thermoelectric cooler (TEC), producing too much heat for the interior of the roll tube. The solution was to add thermally conductive heat straps to draw heat away from the sensor to one of the magnesium end caps on the roll tube, allowing for the camera to still rotate and slide on the FMC mechanism. NIR/SWIR and LWIR lenses replaced the legacy lenses without modification to the roll tube due to barrel and thread-matching incorporated into the custom lenses. Lastly, the existing thermal baffle for the legacy LWIR sensor was modified using wire-Electrical Discharge Machining (wire-EDM) to shorten the height to accommodate a longer LWIR lens and a necessarily altered installation procedure.

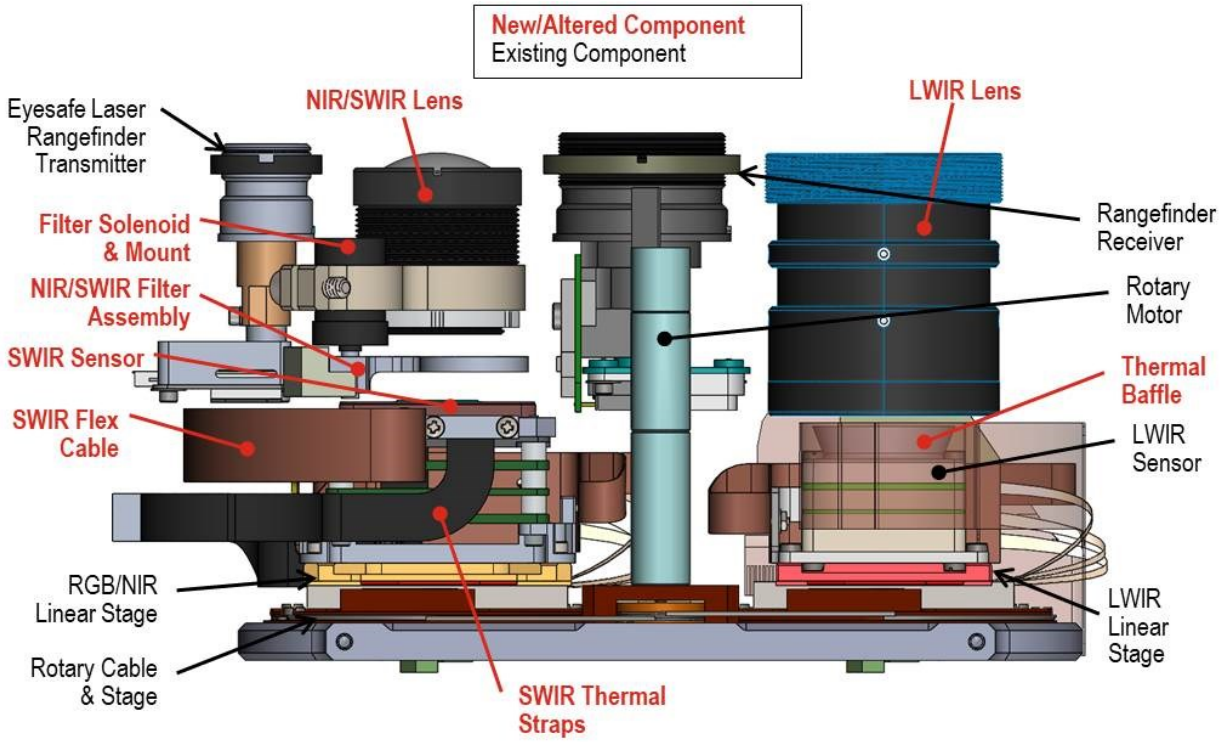

Figure 16. Hardware modifications/additions/replacements to the interior of the roll tube assembly.

Ground Processor Description and Sample Results

NVESD developed the MARINE SCOUT processor for decompressing, viewing, analyzing, quantifying, and mapping imagery from the three MARINE SCOUT infrared sensors. MARINE SCOUT saves sequential images from each camera as time coded loss-less jpeg files, and associated metadata is saved in binary files. In addition, time coded local environmental data needed for the oil depth analysis was collected by an Onset weather station.

Figure 17 shows how the MARINE SCOUT loss-less jpeg files are decompressed and coupled with the metadata. After decompression, the images can be reviewed using the playback feature,

allowing the analyst to choose LWIR, NIR, and SWIR frames of interest. The playback feature is also a valuable tool to quickly determine sensor performance and possible saturation, defocusing, and corrupted images.

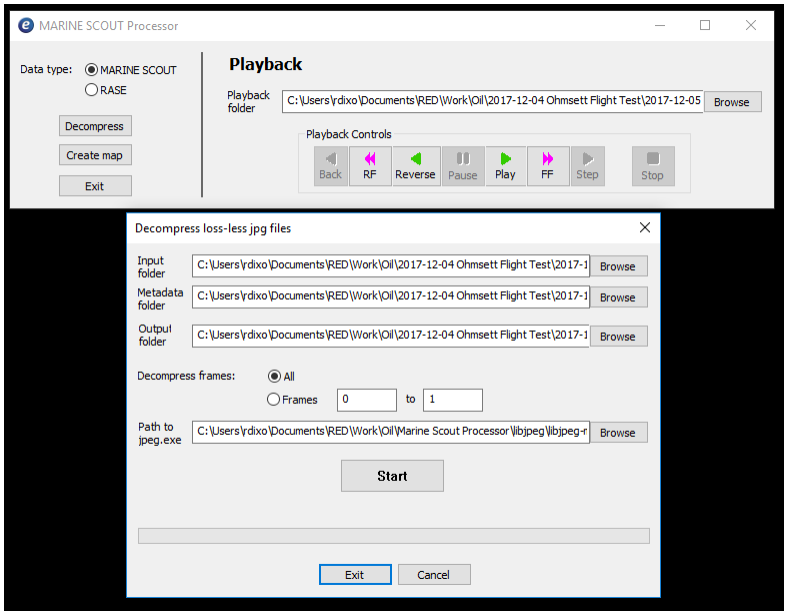

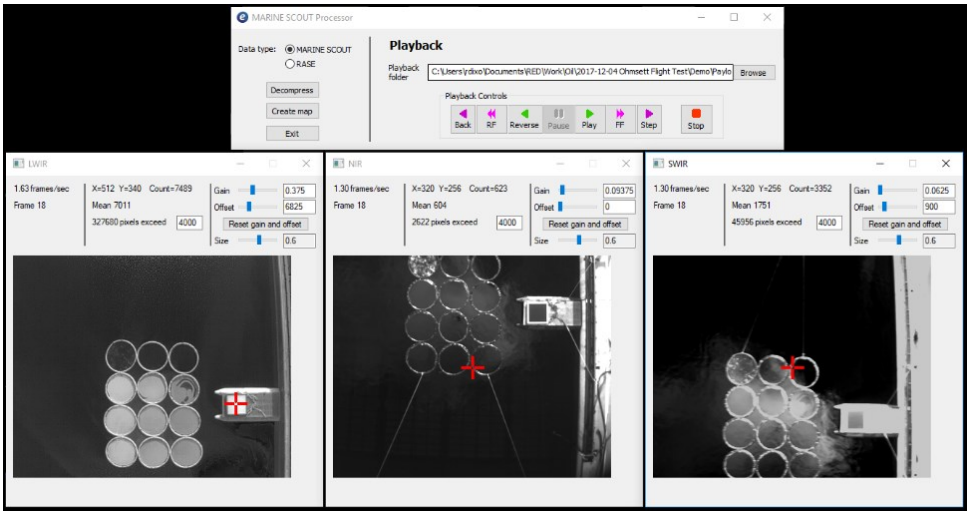

Figure 17. The initial stages of the MARINE SCOUT PROCESSOR showing data decompression and playback.

Before creating maps, the frames of interest are stitched together and the resulting stitched LWIR, NIR and SWIR images are co-registered. The user selects match points to co-register the LWIR, NIR and SWIR, and each match point can be associated with its latitude and longitude for use as a Ground Control Point (GCP). If GCPs are not used the location is determined using metadata, although this method is not as accurate. Mean, median, standard deviation, minimum and maximum

pixel intensities are displayed to provide the analyst a quantitative measure of image quality. The stitched and registered images are shown in Figure 18.

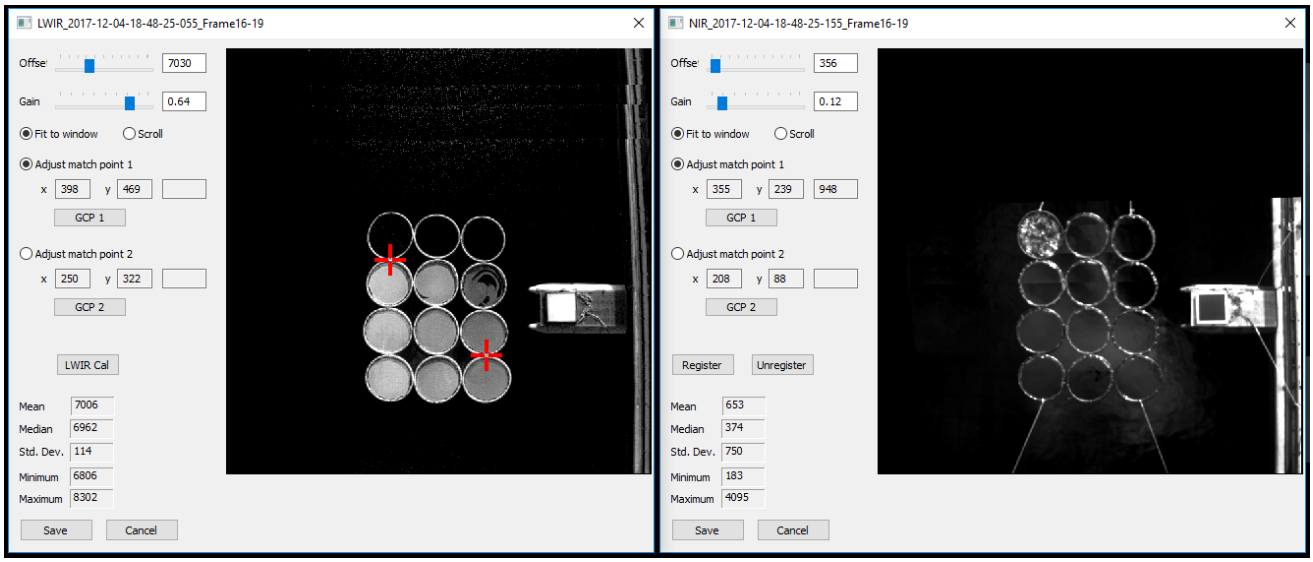

Figure 18. Registered stitched maps can be created for all three sensors and viewed simultaneously.

The next step is to create maps, which can represent counts, temperature, or depth. The existing LWIR camera does not provide a radiometric (temperature) output, so to convert the digital counts to temperature a two-point conversion is done using an in-scene blackbody and the surrounding water as known temperature points. The oil depth is computed using modelled depth equations from Allik, et al.[10] The blackbody and water temperatures have been recorded by the Onset weather station.

The map can be enhanced using color coding, Gaussian or median filters, thresholding and gain adjustments. Statistics are provided to assist in setting the display parameters.

Figure 19 is a sample output showing depth of three crude oils and emulsions. The three crude oils are Alaskan North Slope (ANS), Hoover Offshore Oil Pipeline Systems (HOOPS), and Rock crude. These values are typically within 1-2 standard deviations of the depth of the dispensed oil.

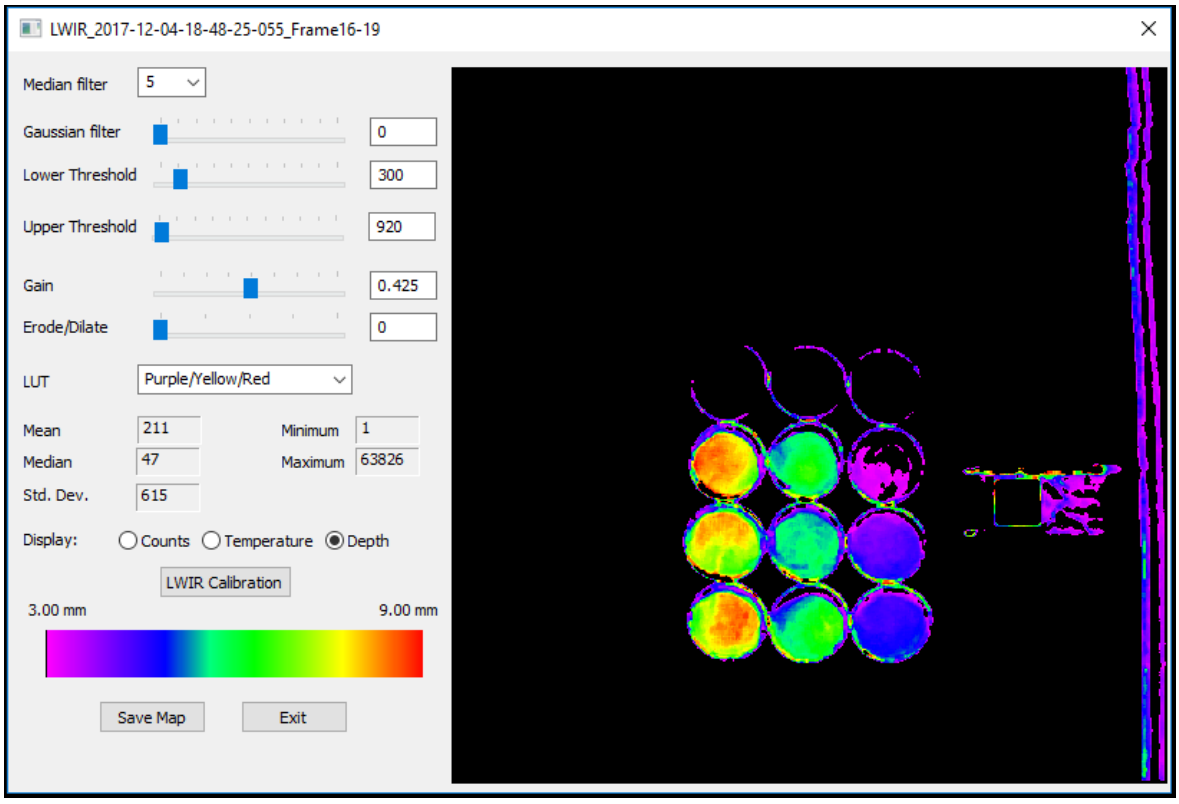

Figure 19. Calibrated LWIR thermal image.

To improve clutter rejection, masks can be generated from the NIR and/or SWIR image, see Figure 20. In this case a mask was created that rejects pixels that have a relatively high intensity in the NIR, using the assumption that oil will have a low reflectivity in the NIR (compared to kelps, seaweed and other vegetation), and therefore low intensity.

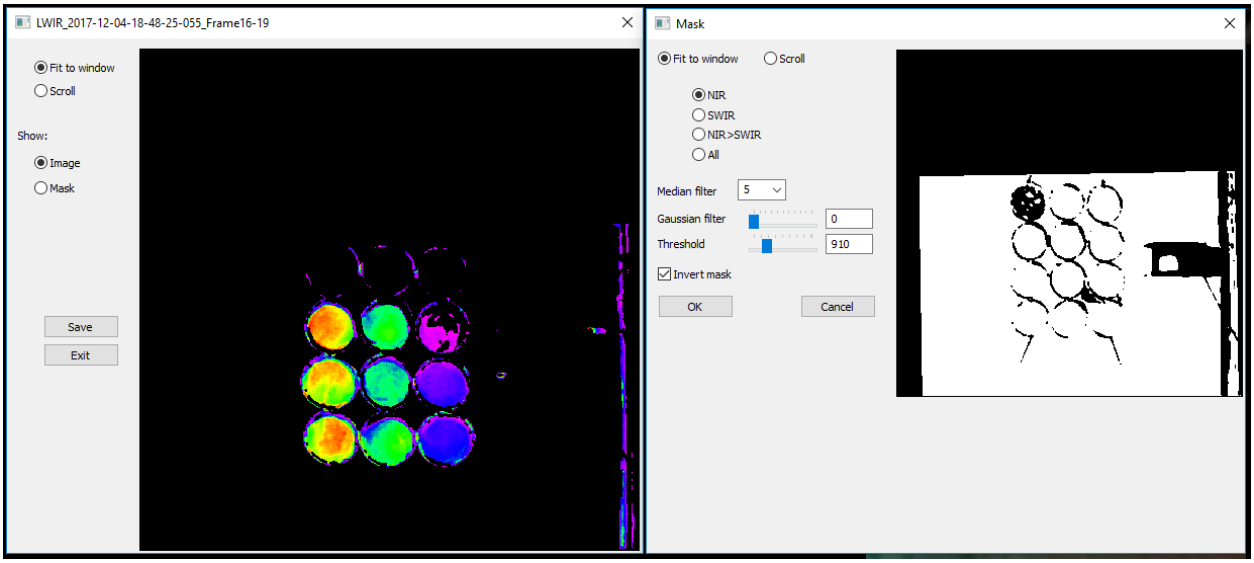

Figure 20. A clutter rejecting mask applied to LWIR map.

Maps can be saved in .kml and .kmz formats for viewing in a variety of mapping applications, see Figure 21.

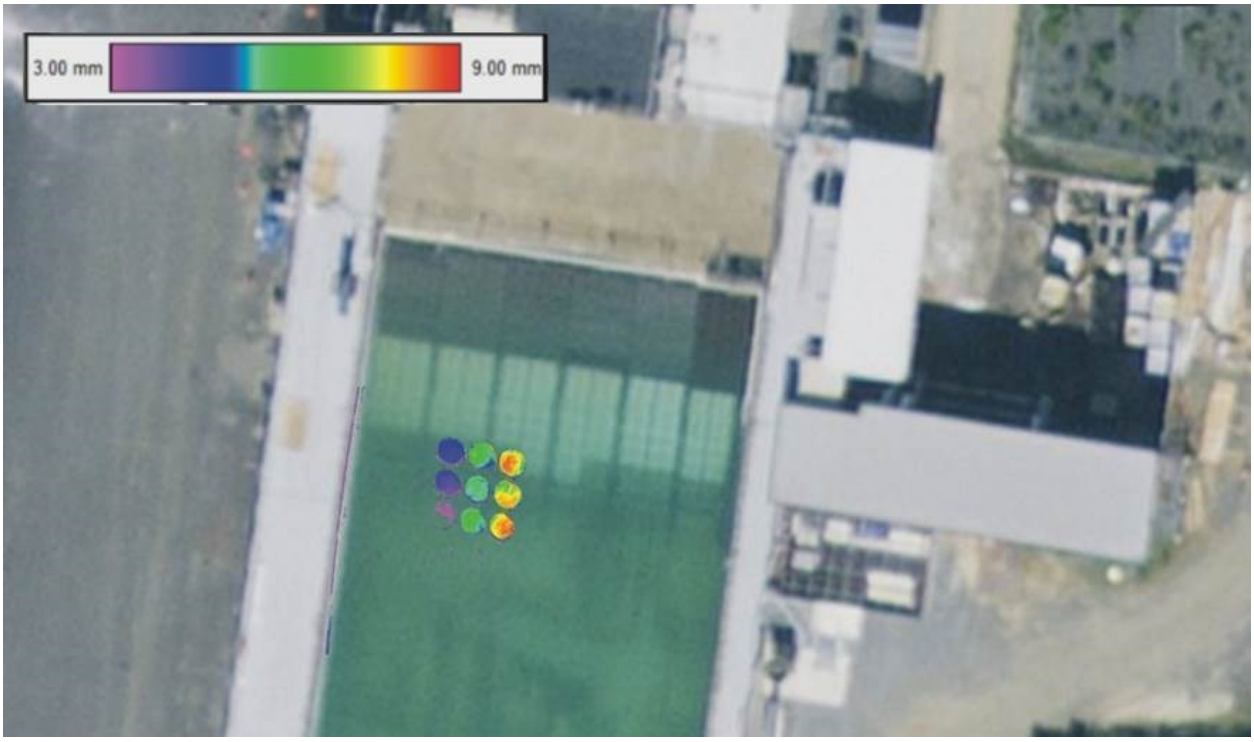

Figure 21. Satellite earth imagery of crude oils with legend showing oil depth.

Outdoor field tests were performed at OHMSETT test facility. This facility afforded an ideal location to evaluate the performance of the sensor payload and ground processing suite, having a good inventory of crude oils, the ability to handle and dispose of oil waste, support equipment, and a highly trained staff. Crude oils and emulsions were contained in a target raft containing surface-floating, 1.5-meter diameter rings with skirts that would contain the oils during windy conditions and minimize oil loss and cross-contamination. The preceding figures in this section portray imagery and processed results collected during this experiment.

Summary and Conclusions

A Government-industry team completed a program supporting the DOI/BSEE that demonstrated a compact, lightweight, multi-spectral airborne sensor payload capable of detecting the presence of oil on water, discriminating oil from false alarms such as kelp forests, and providing a reliable estimate of the thickness of the oil present on the water. Using three spectral bands (LWIR, NIR, and SWIR), the payload is capable of operating in degraded visual conditions and at night as well as daytime. Leveraging a legacy U.S. Army capability, the realized MARINE SCOUT payload is fully compatible with the AeroVironment Puma Small UAS.

Two MARINE SCOUT payloads were fabricated and delivered to the DOI/BSEE. The prototypes were flight tested at multiple U.S. locations, and demonstrated the ability to collect the multi-spectral mosaics of ground-mapped imagery. These digital mosaics were then processed on a ground computer to demonstrate the ability to discriminate oil and measure its thickness.

Recommendations for Future Work

Sensor Improvements

- Upgrade LWIR sensor channel for radiometric (temperature) calibration

Marinization

- Required to support salt spray and saltwater landings
- Achieved by combining new seals, new lubricants, covers and super-hydrophobic coatings
- Fresh water rinse will be required after every water landing
- Some parts may require occasional recoating and/or relubricating
- No major structural modifications required to support AE operation

Additional Refinements to the Heat Transfer Models

- Include the effects of oil evaporation, water currents and waves to the models
- Determine thermal conductivity of oil emulsions
- Determine air convention coefficient for oil-air interface

Turn-Key Operation / Data Collection

- Provide a complete sensor solution with dedicated UAV
- Automate processing (real-time oil detection, ingest weather data in real time to the processor)
- Increase mapping accuracy
- Create maps compatible with vendor and government requirements

References

[1] https://www.bsee.gov/what-we-do/research/oil-spill-preparedness/oil-spill-response-research

[2] M.F. Fingas, "The basics of oil spill cleanup," 3rd edition, CRC Press, ISBN 978-1-4398-6246-9, (2013).

[3] M. Fingas, [Handbook of Oil Spill Science and Technology], Wiley, ISBN 978-0-470-45551-7, (2015).

[4] A.A. Allen, D.H. Dale, Galt, J.A., J.A. Murphy.., "Effective Daily Recovery Capacity (EDRC) Project Final Report," Genwest System and Spiltec, Edmonds, WA, (7 December 2012).

[5] J. Svejkovsky, M. Hess, J. Muskat, T.J. Nedwed, J. McCall, O. Garcia, "Characterization of surface oil thickness distribution patterns observed during the Deepwater Horizon (MC-252) oil spill with aerial and satellite remote sensing", Marine Pollution Bulletin 110, 162-176 (2016).

[6] "ROVs and AUVs Collect Slick Thickness Measurements," The Ohmsett Gazette, (Spring/Summer 2017).

[7] T.H. Allik, R.E. Dixon, M. Roberts, M. Walters, T.J. Soyka, J. Cho, "Enhanced oil spill detection sensors in low-light environments", Proc. SPIE 9827, Ocean Sensing and Monitoring VIII, 98270B (May 17, 2016); doi:10.1117/12.2222064.

[8] T.H. Allik, R.E. Dixon, L. Ramboyong, M. Roberts, P. Zinser, T.J. Soyka, "Enhanced Oil Spill Detection Sensors in Low-Light Environments," OSPR/Chevron Oil Spill Response Technology Workshop, Albert H. DeWitt Officer's Club, Alameda CA, https://www.wildlife.ca.gov/OSPR/Public-Meetings, (25 February 2015).

[9] T.H. Allik, R.E. Dixon, L.V. Ramboyong, M. Roberts, T.J. Soyka, G. Trifon, L. Medley, "Novel Electro-Optic Imaging Technologies for Day/Night Oil Spill Detection", International Oil Spill Conference Proceedings, Vol. 2014, No. 1, pp. 299609, (May 2014).

[10] T.H. Allik, R.E. Dixon, M. Walters, "Remote measurement of thick oil spill depth using thermal imagery," Proc. SPIE 10631, Ocean Sensing and Monitoring X, (25 May 2018); doi: 10.1117/12.2300266; https://doi.org/10.1117/12.2300266.

[11] S. Myhr, G. Ax, J. Gill, L. LeClair, E. Sippel, M. Walters, T.H. Allik, R.E. Dixon, "Mapping and reconnaissance imager, night-enhanced, for sensing of contaminants, oil, and unseen threats (MARINE SCOUT)," Proc. SPIE 10631, Ocean Sensing and Monitoring X, (25 May 2018); doi: 10.1117/12.2303963; https://doi.org/10.1117.12.2303963.

[12] Alaska North Slope (ANS), Exxon Mobile data sheet.

[13] F.P. Incropera, D.P. Dewitt, T.L. Bergman, A.S. Lavine, "Fundamentals of Heat and Mass transfer", 6th ed., John Wiley and Sons, (2007).

[14] W.L. Wolf, G.L. Zissis, The Infrared Handbook (revised edition) ISBN: 0-9603590-1-X, page 3-15 (1993).

[15] M.A. Goforth, G.W. Gilchrist, J.D. Sirianni, "Cloud effects on thermal downwelling sky radiance", Proc. SPIE 4710, Thermosense XXIV, (15 March 2002); doi: 10.1117/12.459570.

[16] M. Luciuk, "Night radiative cooling: the effect of clouds and Relative Humidity", Tech. Print. Retrieved from www.asterism.org/tutorials/tut37%20Radiative%20Cooling. Pdf, (2012).